

Hydride spectroscopy of the diffuse interstellar medium: new clues on the gas fraction in molecular form and cosmic ray ionization rate in relation to H_3^+

BY M. GERIN¹, F. LEVRIER¹, E. FALGARONE¹, B. GODARD², P. HENNEBELLE¹, F. LE PETIT³, M. DE LUCA¹, D. NEUFELD⁴, P. SONNENTRUCKER⁵, P. GOLDSMITH⁶, N. FLAGEY⁶, D. C. LIS⁷, C. M. PERSSON⁸, J. H. BLACK⁸, J. R. GOICOECHEA², K. M. MENTEN⁹

¹*LERMA, Observatoire de Paris, CNRS UMR8112 and ENS*, ²*Centro de Astrobiología (CAB)*, ³*LUTh, Observatoire de Paris, CNRS UMR8102*, ⁴*John Hopkins University*, ⁵*Space Telescope Science Institute*, ⁶*Jet propulsion Laboratory*, ⁷*California Institute of Technology*, ⁸*Earth and Space Sciences, Chalmers University*, ⁹*Max Planck Institute für Radioastronomie.*

The Herschel guaranteed time key program PRISMAS (PRobing InterStellar Molecules with Absorption line Studies)† is providing a survey of the interstellar hydrides containing the elements C, O, N, F and Cl. As the building blocks of interstellar molecules, hydrides provide key information on their formation pathways. They can also be used as tracers of important physical and chemical properties of the interstellar gas that are difficult to measure otherwise. This paper presents an analysis of two sight-lines investigated by the PRISMAS project, towards the star forming regions W49N and W51. By combining the information extracted from the detected spectral lines, we present an analysis of the physical properties of the diffuse interstellar gas including the electron abundance, the fraction of gas in molecular form and constraints on the cosmic ray ionization rate and the gas density.

Keywords: Diffuse interstellar medium, W49N, W51

ÆDiffuse interstellar medium, W49N, W51

1. Introduction

The diffuse interstellar medium occupies a central place in the life cycle of interstellar gas, with its relatively large filling factor of the Galaxy volume. Its structure is sensitive to the large scale forces operating galaxy-wide, including turbulence (partially generated by the differential rotation of the Galaxy), magnetic fields, far UV radiation and cosmic rays. Studying the structure and composition of the diffuse interstellar medium is therefore one of the best means to obtain observational constraints on these phenomena. The Herschel guaranteed time key programme PRISMAS was designed to search for the ground state rotational lines of the main hydrides playing a key role in the interstellar chemistry. Observations were performed in absorption towards distant star forming regions in the galactic plane. Given the excellent sensitivity of the Herschel/HIFI instrument [1], and the large

† Herschel is an ESA space observatory with science instruments provided by European-led Principal Investigator consortia and with important participation from NASA.

Table 1. *Properties of PRISMAS sources*

Name	α (J2000)	δ (J2000)	D kpc	R kpc
SgrA+50	17 45 50.2	-28 59 53	8.4 ¹	0.05
W28A	18 00 30.4	-24 04 00	3.8 ²	4.7
G10.6-0.4(W31C)	18 10 28.7	-19 55 50	4.8 ¹	3.9
W33A	18 14 39.4	-17 52 00	4.0 ¹	4.7
G34.2+0.15	18 53 18.7	+01 14 58	2.0 ³	7.0
W49N	19 10 13.2	+09 06 12	11.4 ¹	7.9
W51	19 23 43.9	+14 30 31	5.4 ⁴	5.8
DR21(OH)	20 39 01.0	+42 22 48	1.5 ⁵	8.4

Columns are source name, equatorial coordinates (J2000), distance from the sun and Galacto-centric distance.

¹ see [2, 3] for the discussion on the distance. ² [3]; ³ [4]; ⁴ Similar distance as G35.20-0.74 which has a comparable radial velocity [5]. ⁵ [6]

line strengths of these lines, this method allows the detection of diffuse interstellar matter along the line of sight with a similar sensitivity as optical and near infrared spectroscopy towards bright early type stars. The main difference is the larger range of Galactic distances along the line of sight, extending to several kiloparsecs across the Galactic Plane. Table 1 summaries the properties of the PRISMAS sources.

2. A short summary of first PRISMAS results

The first observations obtained with Herschel/HIFI confirmed the excellent sensitivity of the instrument, and fully revealed the capabilities of hydride spectroscopy for studying the interstellar medium. The detection of ubiquitous absorption by hydrogen fluoride, HF, and the close similarity with spectra of para water (p-H₂O) [7, 8] and methylidyne (CH) [9] provide a strong confirmation of the use of CH and HF as tracers of diffuse molecular gas. Both species trace molecular gas down to total hydrogen column densities of a few 10^{20} cm⁻², in a regime where the CO rotational line emission is not a proper tracer of the molecular gas [10]. Throughout this paper, we write N_{H} for the total column density of hydrogen, $N(\text{H}_2)$ for the column density of molecular hydrogen, and $N(\text{H I})$ for the column density of atomic hydrogen. The fraction of hydrogen nuclei bound in H₂ (i.e. the *molecular fraction*) is therefore $f(\text{H}_2) = 2 N(\text{H}_2)/N_{\text{H}}$.

The analysis of water vapor spectra is complicated by blending of the diffuse absorption with the strong emission from the background star forming regions resulting in complex profiles combining emission and absorption. An extensive analysis of water line profiles, including the ortho and para ground state lines, shows that water vapor is associated with molecular hydrogen like CH and HF, with an abundance of $\sim 10^{-7}$ [11]. The ortho to para ratio for the diffuse absorbing gas is generally in agreement with the high temperature limit of 3 [12, 11]. Such a behavior is consistent with the expectation from the gas phase formation of water vapor by the dissociative recombination of H₃O⁺.

Among neutral species, the nitrogen hydrides exhibit the unexpected result that NH₂ and NH₃ have similar column densities, while NH was found to be about twice as abundant

as either NH_2 and NH_3 . [13, 14]. NH_2 and NH_3 show a tight correlation while their relation with NH is slightly more dispersed. The precursor ion NH^+ remains undetected.

This latter result comes as another surprise, since many hydride ions have been easily detected with HIFI. This is the case for the hydroxyl ions OH^+ , H_2O^+ , and marginally H_3O^+ . The former two ions present intense absorption over a broad velocity range. Hydroxyl ions can be used as probes of the cosmic ray ionization rate of hydrogen. Indeed, their formation is initiated by the reaction of ionized oxygen O^+ with H_2 . Since the main pathway to O^+ is the charge transfer reaction with H^+ , created by the interaction of cosmic rays with hydrogen, the abundance of hydroxyl ions like OH^+ and H_2O^+ scales linearly with the cosmic ray ionization rate. A surprising result of the HIFI observations was the large excess of OH^+ over H_2O^+ , with a typical $\text{OH}^+/\text{H}_2\text{O}^+$ column density ratio of $\sim 5-6$, which implies that these ions reside in mostly atomic gas, with a fraction of hydrogen in molecular form $f(\text{H}_2)$ smaller than 10 percent [15, 16].

The methyldiyne ion CH^+ also shows strong absorption along the diffuse sight-lines, with many instances of fully saturated profiles across a broad velocity range, while the corresponding lines from $^{13}\text{CH}^+$ remain weak [17, 2]. The combined detection of CH^+ , $^{13}\text{CH}^+$ and sulfanylium SH^+ in the diffuse ISM cannot be explained by standard steady state chemical models driven by UV radiation and cosmic rays, since the main formation paths of these ions involve reactions with endothermicities exceeding several thousand kelvins. However, the recently developed models of Turbulent Dissipation Regions (TDR [18]) explain these results well, which is one of the main successes of PRISMAS program.

Among the other species detected by Herschel, two key intermediates in the chlorine chemistry were discovered, H_2Cl^+ [19, 20] and HCl^+ [21, 22]. Both ions are detected in the diffuse interstellar medium, and have similar abundances reaching a few percent of the total abundance of chlorine, a level higher than current model predictions.

3. The example of the W49N and W51 sightlines

Figure 3 presents examples of HIFI spectra towards W49N and W51. All spectra have been divided by the continuum intensity to emphasize the absorption lines. Except for the C^+ fine structure line at 1.9 THz, all data have been taken in double beam switching mode, ensuring an accurate detection of the submillimeter continuum, and flat baselines. The [CII] spectra were taken using the cold load as comparison source, to avoid possible contamination by extended emission. In both cases, the spectra show a combination of emission and absorption from the background source and pure absorption by the diffuse interstellar gas along the line of sight. In the following, we only discuss the absorption components not associated with the background high-mass star forming region. These correspond to LSR velocity ranges from 30 to 75 kms^{-1} for W49N and from 0 to 48 kms^{-1} for W51.

The molecular column densities calculated for different velocity ranges along the absorption profiles are compared in Figure 3. Different colors correspond to different velocity intervals. Dashed lines show linear trends, while dotted lines indicate quadratic trends. The good correlation, with a correlation coefficient of 0.82, between the two molecules believed to be the most accurate tracers of molecular hydrogen, namely HF and CH is remarkable. HCO^+ and p- H_2O are also well correlated with CH, but with a larger dispersion. For those species, a quadratic trend seems to fit the data slightly better than a linear trend.

The mean ratio between CH and HF is $\sim 3.4 \pm 1.2$ in W49N, and has a somewhat lower value of ~ 2.5 in W51. Given the fluorine elemental abundance of 1.8×10^{-8} [23] and assuming that all fluorine is in HF, the expected HF abundance relative to H_2 is 3.6×10^{-8} ,

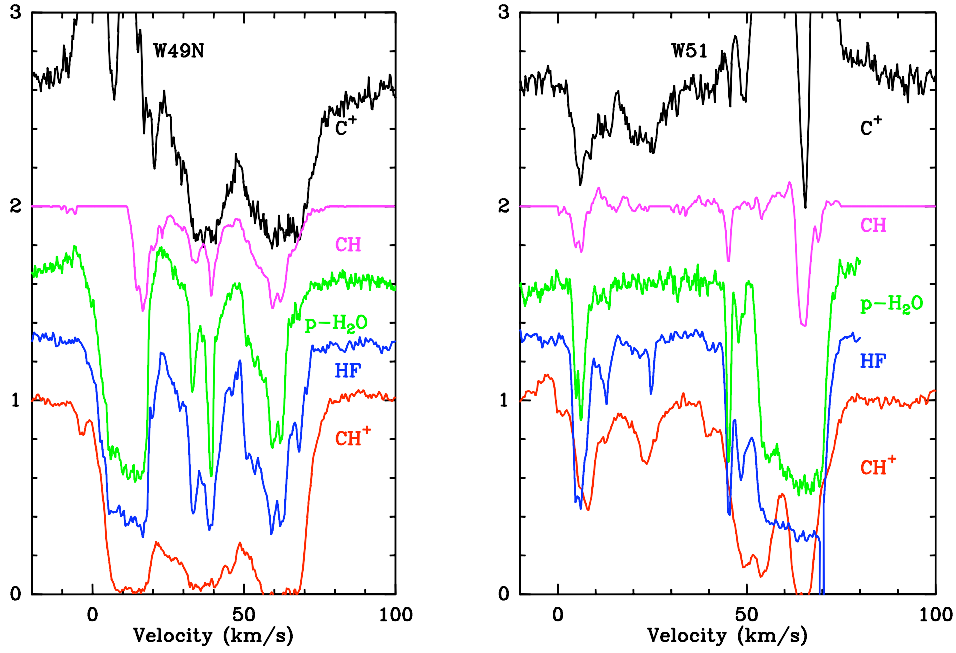


Figure 1. Selection of HIFI spectra towards W49N (Left) and W51 (Right). The spectra have been normalized to the continuum to emphasize the absorption profiles, and shifted vertically to avoid overlap.

which is very close to the mean CH abundance in local diffuse clouds, 3.5×10^{-8} [24], derived for H_2 column densities ranging between $\sim 2 \times 10^{19}$ and $\sim 3 \times 10^{21} \text{ cm}^{-2}$. Possible explanations for the deviation from unity are discussed in [2] and involve some depletion of fluorine, or a higher abundance of CH relative to H_2 in spiral arm clouds than in local diffuse clouds.

The C^+ column follows a different pattern. This is expected since absorption by ionized carbon can be produced both in diffuse atomic and molecular gas, where C^+ is the main reservoir of carbon. C^+ absorption is therefore expected to trace the total hydrogen column density of the regions where C^+ is the dominant form of carbon [25]. PDR models show that C^+ remains the dominant form of carbon up for H_2 column densities up to $1 - 2 \times 10^{21} \text{ cm}^{-2}$ [26, 27] in diffuse and translucent gas with moderate densities. Therefore we expect the C^+ absorption to trace the total column density of hydrogen along the PRISMAS sight-lines. This expectation is confirmed by the looser correlation between C^+ and CH, with many velocity intervals showing a broad range of CH column densities for a similar C^+ column.

The rather loose correlation between CH and C^+ indicates that $f(H_2)$ varies among the different velocity components along the line of sight. To be more quantitative, we have combined the information from CH and C^+ to derive the total hydrogen column density N_H , the column density of molecular hydrogen $N(H_2)$ and the column density of atomic hydrogen $N(HI)$. Assuming a constant abundance of ionized carbon of 1.4×10^{-4} , the C^+ column density is proportional to the total hydrogen column density with $N_H = N(C^+)/1.4 \times 10^{-4}$. Given the range of galacto-centric distances R (see Tab. 1) probed by these measurements and the weak metallicity gradient of the Milky Way [28], this assumption should be correct within 20%. The H_2 column density is derived from CH using the mean abundance in local

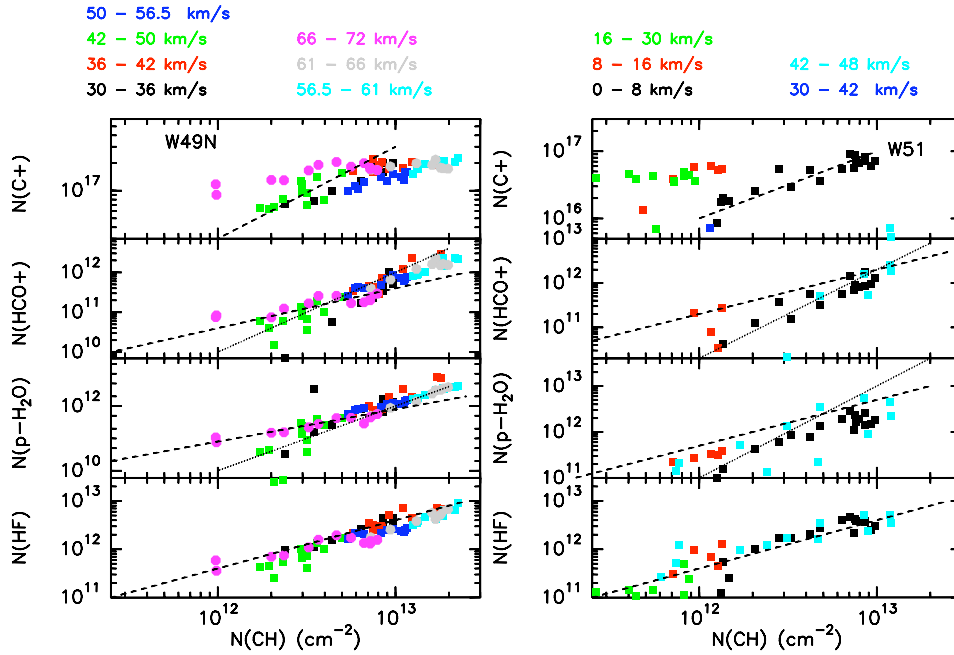


Figure 2. Comparison of the HF, p-H₂O, HCO⁺ and C⁺ column densities with that of CH along the W49N and W51 line of sight. Colors indicate different velocity intervals. Each point correspond to a velocity channel of 0.6 km s⁻¹. Dashed lines show linear trends, while dotted lines indicate quadratic trends.

diffuse clouds : $N(\text{H}_2) = N(\text{CH})/3.5 \times 10^{-8}$, and the column density of atomic hydrogen is simply $N(\text{HI}) = N_{\text{H}} - 2N(\text{H}_2)$.

Figure 3 presents the variation of $N(\text{H}_2)$, $N(\text{HI})$ and $f(\text{H}_2)$ as a function of N_{H} for the W49N and W51 sight-lines. It is interesting to notice that the HI and H₂ column densities have the same order of magnitudes for the different velocity components along both sight-lines, and that the choice of C⁺ and CH abundance does not lead to unrealistic values of the H and H₂ column densities. A remarkable result is the large variation of $f(\text{H}_2)$ along these sight-lines, from almost purely atomic clouds with $f(\text{H}_2) \leq 0.1$ up to mostly molecular clouds with $f(\text{H}_2)$ approaching unity. Another important result is the large spread of $f(\text{H}_2)$ values for the same total hydrogen column density, a finding also obtained by [2] with different assumptions and using ancillary data.

Ongoing observations of the HI 21cm line at high spectral resolution will be used to further constrain the HI content independently and refine this analysis. Given the moderate total column densities of a few 10^{21} cm^{-2} in the various velocity components, the use of C⁺ as the main reservoir of carbon is globally justified. Observations of atomic carbon and carbon monoxide will be used to better establish the carbon budget.

This scatter in physical conditions has some impact on the derivation of the cosmic ray ionization rate from observations of molecular ions. As discussed in [29] an accurate derivation of the cosmic ray ionization rate from measurements of the H₃⁺ column density requires the knowledge of the physical conditions in the diffuse medium, including the degree of ionization, the fraction of gas in molecular form and the average density. The HIFI observations confirm that C⁺ is the major carrier of carbon, and provides most of

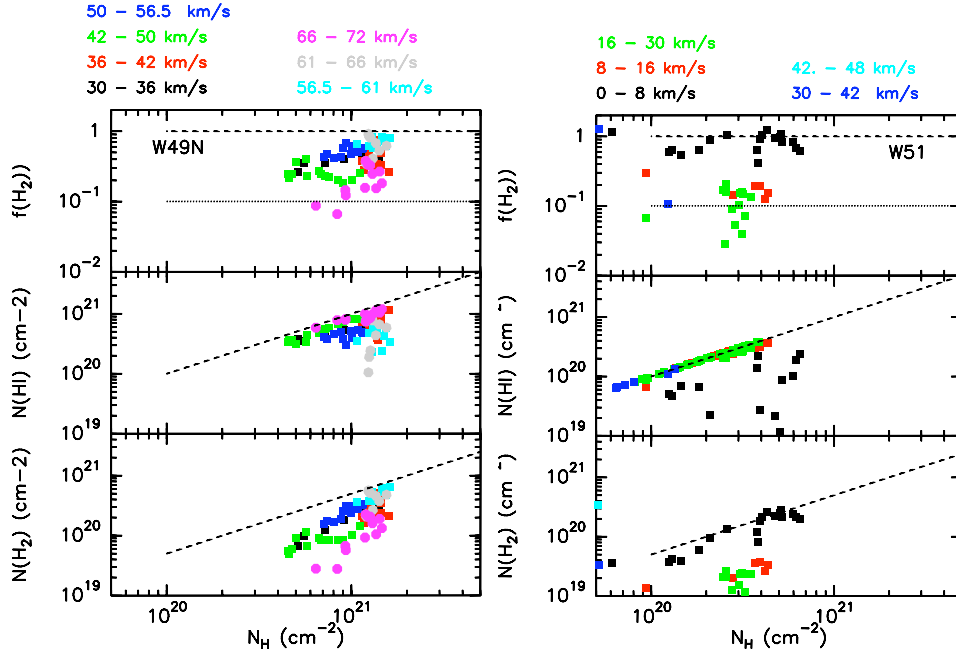


Figure 3. Comparison of the H_2 , HI column densities and of the H_2 fraction, $f(\text{H}_2)$, with the total column density of hydrogen deduced from the C^+ absorption towards the W49N and W51 sight-lines. The H_2 column densities are derived from the CH column densities using a uniform abundance of 3.5×10^{-8} [24]. Colors indicate different velocity intervals. Each point corresponds to a velocity channel of 0.6 km s^{-1} . Dashed lines in the panels for $N(\text{HI})$ and $N(\text{H}_2)$ indicate a slope of unity.

the electrons in diffuse clouds. The variation of $f(\text{H}_2)$ is more surprising, and indicates that it might be necessary to take this variable into account when deriving the cosmic ray ionization rate from H_3^+ . In the following, we discuss how the new generation of models can be used to understand the bias in the analysis of absorption spectra.

4. Insight from models

The formation of molecular clouds can now be modeled using extensive numerical simulations that take into account the interplay of large scale driving forces with a realistic equation of state for the gas, and include magnetic fields. These simulations reproduce the bistable structure of the diffuse interstellar medium well, with a network of dense cold neutral medium structures embedded in warm neutral gas, and a significant fraction of thermally unstable gas [30]. We have used the result of such a magnetohydrodynamic (MHD) simulation to study how the chemical composition of the gas is affected by a complex density structure, as compared to a uniform density medium [31]. In this approach, the chemistry is solved in a post-processing step using the Meudon PDR code [32] along a series of sight-lines through the chosen structure. Since the Meudon PDR code is one dimensional, shadowing effects are present behind opaque structures. To minimize this effect, the computations have been performed along two orthogonal directions and combined based on a criterion of maximum illumination. Fig. 4 presents the predicted spatial distributions of H_2 , CH, C_2 and H_3^+ , while Fig. 5 shows the resulting correlations between the H_2 column

density and the CH, C₂ and H₃⁺ column densities. The lines of sight parallel to the X axis are plotted with squares and those parallel to the Y axis with circles. The color indicates the mean density along the line of sight. As discussed by [31], the temperature structure of the MHD model is very similar to the temperature derived from the PDR code which is computing more accurate heating and cooling rates. All calculations have been performed with a cosmic ray ionisation rate of $\zeta_0 = 5 \times 10^{-17} \text{s}^{-1}$, the default value of the Meudon PDR code.

These figures show the excellent correlation of CH with H₂, with a mean abundance ratio very similar to that observed in the diffuse ISM. C₂ is almost as good a tracer of the H₂ column density as CH, and is spatially well correlated with H₂. Therefore the gas densities derived from the analysis of the C₂ excitation are likely to be well representative of the bulk of the molecular gas.

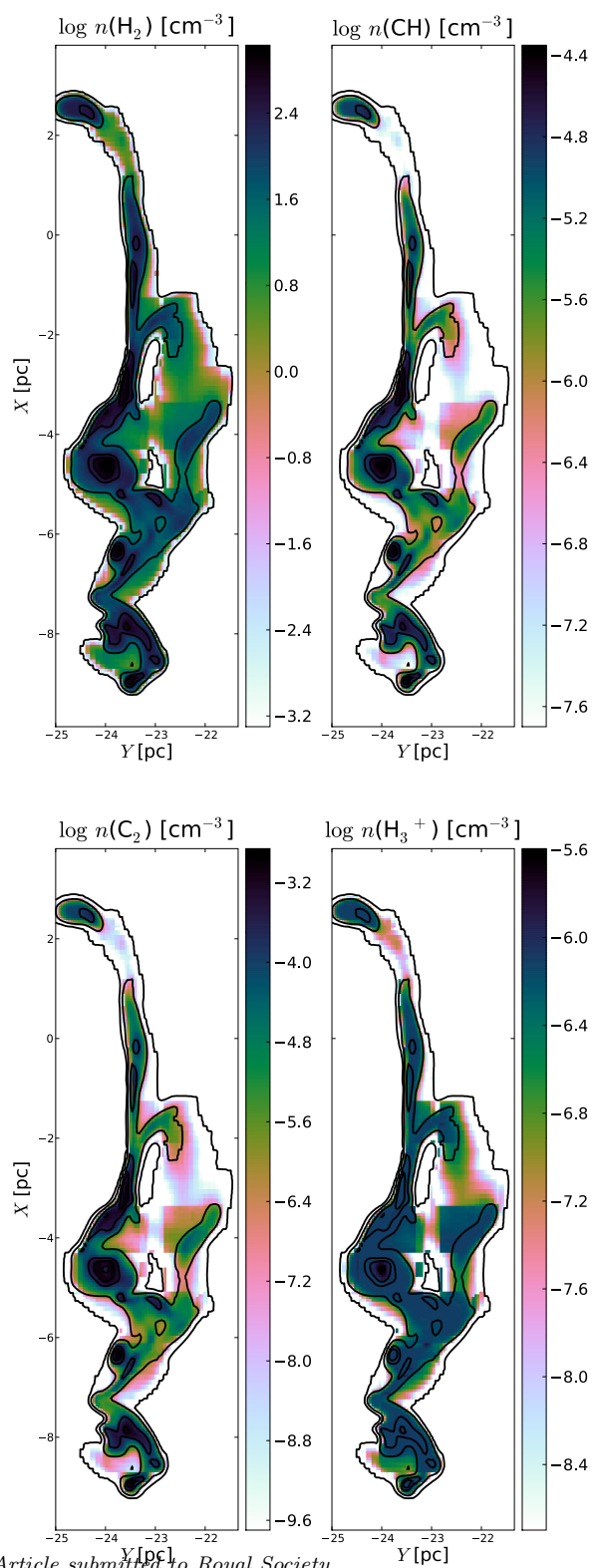
As explained by [29], H₃⁺ is expected to be simply related with H₂ since the cosmic ray ionization rate ζ can be expressed as a function of the H₂ and H₃⁺ densities:

$$\zeta = kx(e)n_{\text{H}}n(\text{H}_3^+)/n(\text{H}_2) \sim kx(e) \langle n_{\text{H}} \rangle N(\text{H}_3^+)/N(\text{H}_2). \quad (4.1)$$

In this formula k is the H₃⁺ dissociative recombination rate and depends on the kinetic temperature. This formula is expected to be valid in diffuse gas where the dissociative recombination with electrons is the main destruction mechanism of H₃⁺. The PDR models were performed with a single value of the cosmic ray ionization rate, and can be used to check the validity of the derivation of ζ from H₃⁺ observations. As expected, the H₃⁺ column densities are slightly larger for sight-lines with lower average density. The dispersion in H₃⁺ column densities for H₂ column density of $\sim 3 \times 10^{20} \text{cm}^{-2}$ is larger than expected. Because of the complex structure along the line of sight, replacing the local H₂ and H₃⁺ densities by the column densities integrated along the line of sight introduces a systematic error in the derivation of the cosmic ray ionization rate.

To evaluate this bias, we have compared the input value of the cosmic ray ionization rate used in the simulation, $\zeta_0 = 5 \times 10^{-17} \text{s}^{-1}$, with ζ values determined using Eq 4.1 from [29]. Densities (including electron densities) are calculated by the PDR code. The electron temperature is assumed to be equal to the gas kinetic temperature, which is also computed by the PDR code. We distinguish between the local values ζ_{local} determined with the local densities and temperature, $\zeta_{\text{local}} = kx(e)n_{\text{H}}n(\text{H}_3^+)/n(\text{H}_2)$ and the values derived from the column densities integrated along a line of sight, $\zeta_{\text{LOS}} = \langle kx(e)n_{\text{H}} \rangle N(\text{H}_3^+)/N(\text{H}_2)$. Note that we use an average value for the rate of dissociative recombination of H₃⁺ since this rate depends on the temperature.

Fig. 6 presents a map of the $\zeta_{\text{local}}/\zeta_0$ ratio using the modeled H₃⁺ and H₂ densities. While this ratio approaches unity in the densest regions, ζ_{local} is clearly underestimated in the more diffuse regions, with typical values of $\zeta_{\text{local}}/\zeta_0$ near 0.5, and reaching 0.2 in the most diffuse regions. Since observations only provide the molecular column densities, we have computed the H₃⁺ and H₂ column densities across the simulation, to better match the models to the observations. The right side of Fig. 6 presents the comparison of the determinations of ζ_{LOS} along sight-lines through the simulation, i.e. using the H₂ and H₃⁺ column densities, with the ensemble of the local determinations ζ_{local} and its mean. For each sight-line, we compute the mean and standard deviation of $\zeta_{\text{local}}/\zeta_0$ plus the LOS value $\zeta_{\text{LOS}}/\zeta_0$. The red dots show the mean and the 1 σ uncertainties on each side of the mean. The dashed line shows the expected slope of unity. The points cluster around this line, but with a large scatter. Furthermore, very few determinations agree with the input value. Therefore, this simple analysis seems to underestimate the true value of the cosmic



Article submitted to Royal Society

Figure 4. Predicted distributions of H_2 , CH , C_2 and H_3^+ . CH and C_2 closely follow H_2 .

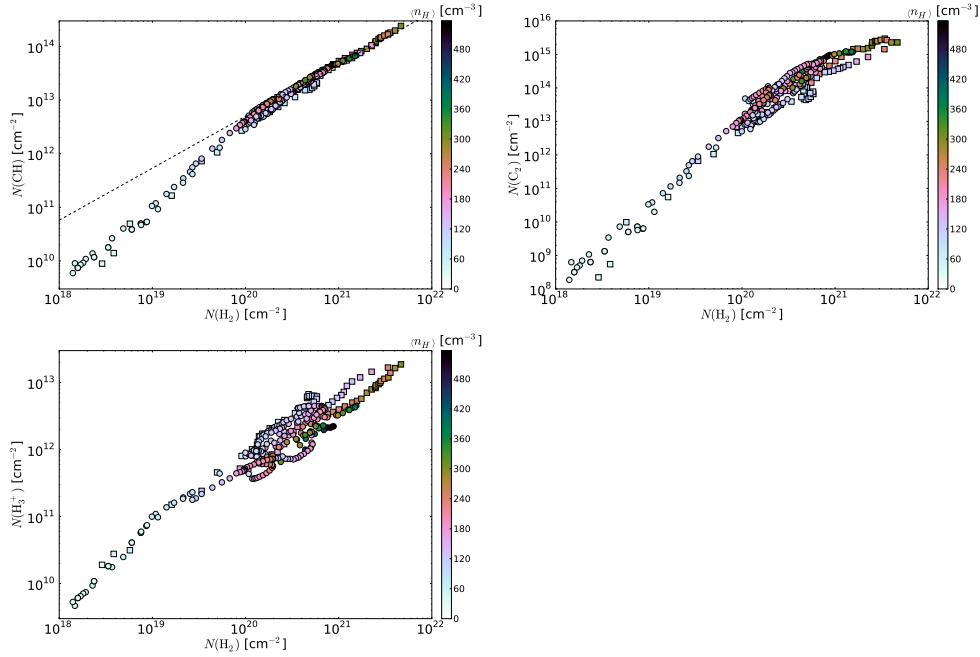


Figure 5. Correlations between the H_2 column density and the CH , C_2 and H_3^+ column densities. The lines of sight parallel to the X axis are plotted with squares and those parallel to the Y axis with circles. The color indicates the mean gas density along the line of sight. The mean trend relating the observed CH and H_2 column densities found by [24] is shown with a dotted line in the CH panel.

ray ionizing rate. Furthermore, the large influence of the local physical conditions implies that a rather large sample of measurements is needed to obtain an accurate determination of ζ .

5. Conclusion

The full access to the submillimeter and far infrared spectral range provided by the Herschel Space Observatory has enhanced our vision of the diffuse interstellar medium, by providing new tracers of its structure and chemistry. Comparing this information with state of the art models of the interstellar medium allows an assessment of our current picture, and helps to establish new directions of research. In this framework, it is interesting to perform numerical simulations combining chemistry and dynamics. Such simulations can be used to assess the bias inherent in the extraction of the chemical information from absorption spectra. They reproduce the good correspondence between CH (and to a lesser extent C_2) with H_2 , as inferred from the direct observations. For the case of H_3^+ , we show that the simple formula commonly used to derive the cosmic ray ionization rate from the H_3^+ column density seems to underestimate slightly the true value of ζ , and presents large statistical fluctuations due to the complex structure of the diffuse interstellar medium.

HIFI has been designed and built by a consortium of institutes and university departments from across Europe, Canada and the United States under the leadership of SRON Netherlands Institute for Space Research, Groningen, The Netherlands and with major contributions from Germany, France and the US. Consortium members are: Canada: CSA, U. Waterloo; France: CESR, LAB, LERMA, IRAM;

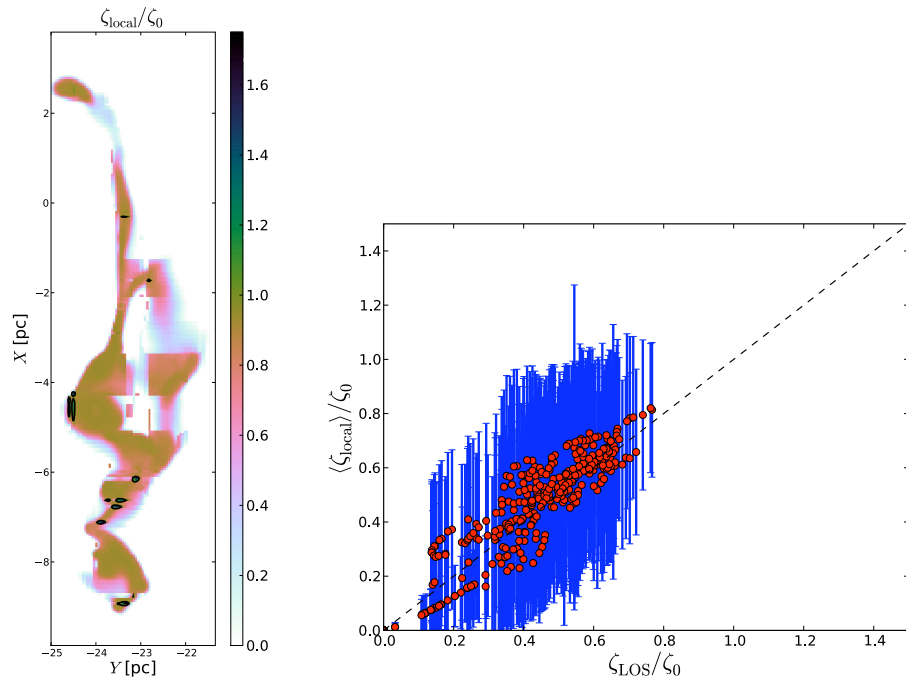


Figure 6. Left: Maps of the cosmic ray ionization rate ζ derived from the H_3^+ density using Eq. 4.1, normalized by the cosmic ray ionization rate ζ_0 used in the simulation ($5 \times 10^{-17} \text{ s}^{-1}$). The contour indicates a ratio of unity. Right: Comparison of the estimations of ζ using the line of sight column densities, with the values along the line of sight. The dashed line shows a slope of one. The estimations of ζ show a large scatter around the value but the linear trend is preserved.

Germany: KOSMA, MPIfR, MPS; Ireland, NUI Maynooth; Italy: ASI, IFSI-INAF, Osservatorio Astrofisico di Arcetri-INAF; Netherlands: SRON, TUD; Poland: CAMK, CBK; Spain: Observatorio Astronómico Nacional (IGN), Centro de Astrobiología (CSIC-INTA). Sweden: Chalmers University of Technology - MC2, RSS & GARD; Onsala Space Observatory; Swedish National Space Board, Stockholm University - Stockholm Observatory; Switzerland: ETH Zurich, FHNW; USA: Caltech, JPL, NHSC. MG, FL, EF, PH and MDL acknowledge support from CNES and from the CNRS/INSU program PCMI. The chemical modeling is partly funded by the grant ANR-09-BLAN-0231-01 from the French *Agence Nationale de la Recherche* as part of the SCHISM project.

References

- [1] de Graauw T. et al. 2010, A&A 518, L6
- [2] Godard B. et al. 2012, A&A 540, A87
- [3] Fish V., Reid M. J., Wilner D.J., 2003, ApJ 587, 701.
- [4] Sato M., Reid M.J., Brunthaler A., Menten K.M., 2010, ApJ 720, 1055
- [5] Zhang B., Zheng X.W., Reid M.J. et al., 2009, ApJ 693, 419.
- [6] Rygl K.L.J., Brunthaler A., Sanna A. et al. 2011, arXiv:1111.7023.
- [7] Neufeld D. et al., 2010, A&A 518 L108
- [8] Sonnentrucker P. et al., 2010, A&A 521 L12.
- [9] Gerin M. et al., 2010b, A&A 521 L16
- [10] Liszt H.S., Pety J., 2012, A&A in press, arXiv 1202.6523.
- [11] Flagey N. et al., 2012, in prep.

- [12] Lis D. et al. 2010 A&A 521 L26
- [13] Persson C. et al., 2010, A&A 521, L45.
- [14] Persson C. et al., 2012 A&A submitted.
- [15] Gerin M. et al., 2010a, A&A 518 L110.
- [16] Neufeld D. et al., 2010, A&A 521 L10
- [17] Falgarone E. et al., 2010, A&A 521 L15.
- [18] Godard B., Falgarone E., Pineau des Forêts G., 2009, A&A 495, 847
- [19] Lis D. et al. 2010 A&A 521 L9
- [20] Neufeld D., Roueff E., Snell R.L. et al., 2012, arXiv 1201.2941
- [21] De Luca M. et al., 2012, ApJ letter in press.
- [22] Gupta H., Drouin B.J., Pearson J.C., 2012, ApJ Letter in press.
- [23] Snow T.P., Destree J.D., Jensen A.G., 2007, ApJ 655, 295
- [24] Sheffer Y., Rogers M. Federman S.R., et al., 2008, ApJ 687, 1075
- [25] Falgarone E., et al. 2010 A&A 518, L118.
- [26] Visser R., van Dishoeck E.F., Black J.H., 2009, A&A 503, 323.
- [27] Le Petit F., Nehmé C., Le Bourlot J., Roueff E., 2006, ApJ suppl 164, 506.
- [28] Daffon, S. & Cunha, K. 2004, ApJ, 617, 1115
- [29] Indriolo N. & McCall B.J., 2012, ApJ 745, 91.
- [30] Audit E., Hennebelle P., 2010, A&A 511, A76.
- [31] Levrier F. et al. 2012 A&A submitted.
- [32] Le Petit F., Barzel B., Biham O., et al., 2009, A&A 505, 1153.